International Journal of Nanoelectronics and Materials
IJNeaM
ISSN 1985-5761 | E-ISSN 2232-1535

A Comparative Study of Fused Filament Fabrication Using Recycled Polystyrene and Commercial High-Impact Polystyrene

Ng Hue Thung Calista[a,b], Seong Chun Koay[a,b,*], Ming Yeng Chan[c], Chen Hunt Ting[a,b] , and Wong Yen Myan Felicia[d]

[a]*Department of Mechanical and Materials Engineering, Lee Kong Chian Faculty of Engineering and Science, Universiti Tunku Abdul Rahman, Kajang, Malaysia*
[b]*Centre for Sustainable Mobility Technologies, Universiti Tunku Abdul Rahman, Sungai Long Campus, Bandar Sungai Long, 43000 Kajang, Malaysia*
[c]*Faculty of Engineering and Technology, Centre for Advanced Materials, Tunku Abdul Rahman University of Management and Technology, Kuala Lumpur, Malaysia*
[d]*College of Future Technology, Base of Red Bird Mphil, Hong Kong University of Science and Technology (Guangzhou), Nansha, Guangzhou, China*
**Corresponding author. Tel.: +603-9086-0288; fax: +603-91908868; e-mail: koaysc@utar.edu.my*

Received 15 September 2023, Revised 1 October 2025, Accepted 27 October 2025

ABSTRACT

Discarded expanded polystyrene (EPS) poses significant environmental challenges due to its accumulation in landfills and resistance to degradation. Upcycling EPS into 3D-printable recycled polystyrene (rPS) filament for use in fused filament fabrication (FFF) shows a promising sustainable solution. This study explores the mechanical recycling of EPS into rPS resin, which is then extruded into 3D-printable filament using a 3DEVO filament maker. A key focus is on studying the filament's properties and the properties of its printed specimen. Filament diameter was monitored in real-time during extrusion using DevoVision software. The results showed that the rPS filament achieved an average diameter of 1.75 mm with a standard deviation of $\pm 0.03\ mm$ when extruded at 200 $°C$. Extrusion at temperatures above 200 $°C$ resulted in filament diameters exceeding 1.75 mm. Specimens printed with rPS filament exhibited higher tensile strength, tensile modulus, and elongation at break, but lower impact strength compared to those printed with commercial high-impact polystyrene (HIPS) filament. Micrographs show that HIPS is a more ductile material, which contributes to its better impact strength. However, due to poor layer adhesion during printing, it exhibited lower tensile properties. The onset and maximum decomposition temperature of rPS did not show a significant change during the recycling process from EPS to filament. The onset decomposition temperature was above printing temperature, thus it did not limit the use of rPS for FFF printing applications. Despite HIPS displaying greater thermal stability, rPS still demonstrates strong potential as a sustainable printing material, and its applications include printing prototypes and serving as a support material in 3D printing, since it can be dissolved in acetone.

Keywords: *Recycled polystyrene, High-impact polystyrene, Fused filament fabrication, 3D printing, Additive Manufacturing*

1. INTRODUCTION

Fused Filament Fabrication (FFF) is an additive manufacturing process where thermoplastic filament is fed through a heated nozzle that melts the material. The nozzle moves along precise paths, depositing the molten filament layer by layer on a build platform. As each layer cools, it solidifies, and the next layer is extruded on top, gradually forming the final object. This technology is also known as Fused Deposition Modeling (FDM), a trademarked term by Stratasys [1]. FFF is widely used due to its simplicity, affordability, and versatility, making it popular for prototyping, education, and low-volume production. Researchers have extensively explored FFF for medical, civil, space, automotive, and many other applications over the last two decades [2]. Grand View Research's market analysis report indicates that technological advancements, cost-effectiveness, and expanding applications across industries are driving significant growth in the FFF 3D printing market. The global FFF market size was valued at approximately $1.7 billion in 2023 and is projected to grow at a compound annual growth rate (CAGR) of 21.8% from 2024 to 2030 [3]. As the FFF 3D printing market grows, research and development in FFF printing material will become crucial to support this growth, with a focus on varying material choices, optimizing material properties, and sustainability to meet diverse application needs.

Expanded Polystyrene (EPS) is a thermoplastic foam material widely used in packaging and insulation applications. It consists primarily of polystyrene beads, which are expanded with a gaseous blowing agent. The expansion process allows EPS to achieve a volume increase of up to 50 times its original size, resulting in a lightweight yet strong material that is approximately 98% air [4]. Due to its high transport cost for recycling, most post-consumer EPS ends up in landfills, leading to environmental pollution [5]. According to INTCO Recycling [6], it reduces the transport cost by recycling EPS through machinery that crushes the EPS into pieces and then melts and compacts it into blocks. EPS waste is often available at little to no cost, making recycled polystyrene (rPS) production significantly cheaper than creating virgin polystyrene, which is energy-intensive and expensive. Converting rPS from EPS into 3D

printable material is a sustainable approach that shows upcycling by transforming discarded materials into high-value products, aligning with circular economy principles and diverting waste from landfills. Additionally, upcycling EPS into 3D printing filaments reduces carbon emissions compared to manufacturing virgin materials, contributing to a smaller environmental footprint, allows industries to achieve cost savings, and promotes advancements in technology. With the increasing market demand for sustainable solutions, rPS can expand further within the industry. Based on research, rPS shows certain limitations, such as brittleness of the material can cause filament breakage, leading to incomplete prints and low mechanical strength of the printed part due to poor adhesion within the printed layers [4-5]. Filament diameter consistency is crucial for FFF printing, as deviations from standard size can lead to clogging if the diameter is too large, which causes printing failure, or under-extrusion if it is too small, which can negatively affect the structural integrity of the printed part. A significant gap exists in the literature regarding the extrusion temperature for rPS, particularly the monitoring and control of filament diameter. This research aims to fill this gap by investigating the relationship between filament diameters during extrusion and other properties of rPS printed parts.

This study focuses on a comprehensive comparison between commercial High-Impact Polystyrene (HIPS) and rPS filament derived from EPS waste, as well as the printed part produced using both filaments. This research initially evaluates the filament properties of rPS produced at different processing temperatures. The comparative study focused on thermal properties of both filaments and the mechanical properties, such as tensile properties and impact strength, of the printed parts produced using both filaments. Morphological characteristics of the fractured parts were also studied to evaluate the structural integrity and material characteristics that correlate with the mechanical properties of the printed parts. The findings will contribute to the upcycling of materials into 3D printing feedstock, support circular economy initiatives, and expand the application scope of rPS in additive manufacturing.

2. METHODOLOGY

2.1. Raw Materials

The process began with the collection of EPS waste, sourced from post-consumer packaging materials, disposable containers, and insulation foam around Sungai Long City, Kajang, Selangor. Proper collection ensured a clean supply of raw material, maintaining the quality of the recycled resin. The HIPS filament used for comparison is from the brand FABBXIBLE, with a diameter of 1.75 mm and a tolerance of ± 0.05 mm. The recommended printing parameters include a nozzle temperature range of 220°C to 250°C and bed temperature between 80°C and 100°C for optimal adhesion and layer bonding.

After collection, the EPS was manually broken into smaller pieces, measuring approximately 5 cm × 5 cm × 5 cm. This step reduced the bulkiness of the foam, making it easier to handle in subsequent processes. The EPS pieces were then heated in an oven at 130°C for about 10 minutes to achieve densification. This step removed any residual moisture and air in the EPS. The densified EPS pieces were then further shredded into smaller crumbs using a PULLIAN Power Crushing Machine (Model: A-150), with a 6mm sieve mesh size. Figure 1 shows the overall process of printed specimens using rPS from EPS waste materials.

Figure 1. Process flow chart of printed specimens using rPS from EPS waste materials.

2.2. Preparation of rPS Pellets

The densified EPS crumbs were processed using a COLLIN TEACH-LINE E20T single-screw extruder operating at a controlled barrel temperature of 180°C with a screw rotation speed of 30 rpm. This extrusion process produced a homogenized recycled PS extrude, which was subsequently pelletized using a COLLIN TEACH-LINE Strand Pelletizer CSG-171-T to obtain uniform pellets with an average length of 2.06 mm, as shown in Figure 2. Prior to filament extrusion, the rPS pellets were subjected to a 12-hour drying in a convection oven maintained at 60°C to remove residual moisture.

Figure 2. rPS pellets.

2.3. Preparation of rPS Filament

The filament production process began by feeding recycled PS pellets into a 3DEVO Composer 350 Filament making machine. Extrusion was performed at different temperatures 190°C, 200°C, and 210°C using a screw speed of 5 rpm. During extrusion, the filament diameter was monitored in real time using DevoVision software, which recorded the filament diameter over the processing time. This automated feedback system ensured consistent filament dimensions by self-adjusting spooling speed to maintain tolerances.

2.4. 3D Print of Specimens

The tensile and impact test specimens in accordance with ASTM D638 Type IV and ASTM D6110 standards were designed using SOLIDWORKS 2024 and then sliced with PrusaSlicer v2.9.0 before being exported as standard tessellation language (.STL) files for printing. All specimens were printed using a BIQU B1 3D printer with the printing parameters as summarized in Table 1.

Table 1 3D printing parameters

Parameters	Value	Unit
Nozzle diameter	0.8	mm
Nozzle temperature	210	$°C$
Bed temperature	90	$°C$
Layer height	0.32	mm
Flow	100	%
Fill angle	45	deg
Fill density	100	%
Print speed	60	mm/s

To ensure good bed adhesion, a heated print bed at 90°C and a 0.8 mm diameter nozzle were used, with a layer height of 0.32 mm. The optimal nozzle temperature of 210°C was identified through a temperature tower test, evaluating temperatures ranging from 180°C to 230°C. For both HIPS and rPS specimens, a 45° fill angle and 100% flow rate/infill density were applied to maximize mechanical performance. To overcome warping issues observed with rPS, the print bed was pre-treated with a glue stick prior to printing.

2.5. Testing and Characterization

2.5.1. Tensile and Impact Testing

For analyzing filament properties, the diameter was measured in real-time during filament production using DevoVision. The obtained data were used to calculate the average diameter, standard deviation, and skewness using MICROSOFT Excel 2021.

Tensile properties were evaluated using a SHIMADZU Universal Testing Machine AGS-X Series following ASTM D638 standard. Eight specimens were tested for each material at a crosshead speed of 5 mm/min with a load cell size of 100kN. The test measured tensile strength, tensile modulus, and elongation at break.

Impact strength was tested using the GOTECH Pendulum Impact Tester (Model: GT-7045-MD) following ASTM D6110 standard. Notched specimens were tested under 1J hammer load conditions to evaluate material toughness and energy absorption capacity.

2.5.2. Scanning Electron Microscopy Analysis (SEM)

The fractured specimens were examined using a HITACHI Field Emission Scanning Electron Microscope (FESEM) (Model: S-3400N) at magnifications of 100 × and 800 × to evaluate surface morphology and interlayer adhesion characteristics. Prior to analysis, the specimens were sputter-coated with a thin layer of gold-palladium to enhance conductivity. Imaging was performed at an accelerating voltage of 15 kV.

2.5.3. Thermogravimetric Analysis (TGA)

The thermal properties of rPS pellets, rPS filament, and HIPS filament were evaluated using PERKINELMER® Simultaneous Thermal Analyzer (STA) 800 following ASTM E1131 standard. Samples were heated from 30°C to 650°C at 10°C/min under nitrogen purge (50 mL/min), with mass loss and derivative thermogravimetric (DTG) curves recorded. The onset degradation temperature (T_d onset) indicating the initial temperature of significant material decomposition, and the maximum decomposition temperature (T_d max) corresponding to the peak decomposition rate, were observed in the DTG analysis.

3. RESULTS AND DISCUSSION

3.1. Filament Inspection

Figure 3 shows the average diameter and skewness of the rPS filament extruded at different processing temperatures. The commercial 3D printing filament, such as the HIPS filament used in this research, has a standard diameter of 1.75 mm with a tolerance of $\pm$0.05 mm. Among the three temperatures, 200°C produced filaments within the standard diameter of 1.75 $\pm$ 0.05 mm, while 210°C slightly exceeded the standard. However, the rPS filament extruded at 190°C showed an average diameter lower than the standard. The skewness of the average filament diameter provides insight into the distribution of measurements. A positive skewness, as observed in rPS extruded at 210°C, suggests that most filament diameters are slightly below the average. In contrast, a negative skewness, seen in rPS extruded at 190°C and 200°C, indicates that the majority of diameter measurements are slightly above the average. In common industry practice, a skewness value within $\pm$0.5 is considered ideal. The rPS filaments extruded at the three different temperatures all exhibited skewness values within this range, indicating a stable extrusion process with a well-centered diameter distribution.

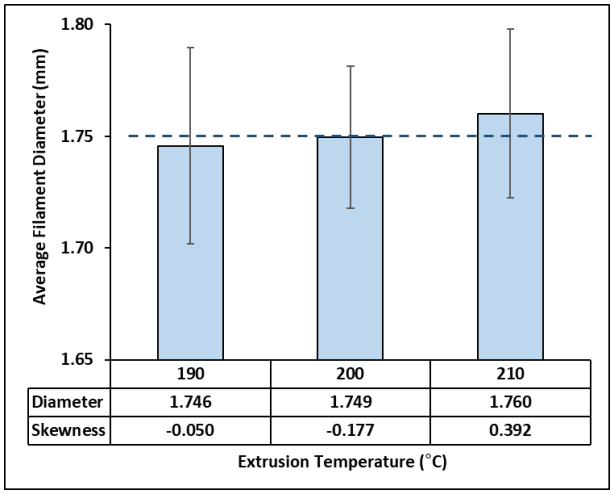

Figure 3. Average diameter and skewness of rPS filaments extruded at different processing temperatures.

At 190°C, the filament exhibited a slightly smaller diameter along with a higher standard deviation. This is likely due to insufficient melting, which may have caused uneven material flow and under-extrusion [7]. The rPS filament extruded at 210°C produced a slightly thicker diameter, which is not ideal for the 3D printing process, as it may lead to nozzle clogging during extrusion. The selection of 200°C as the optimal filament extrusion temperature is justified by its average diameter being closest to the standard, along with a smaller deviation, indicating better consistency in filament production. Hamat et al. [8] and Senkerik et al. [9] investigated the effect of extrusion parameters on the diameter of filaments produced using polylactic acid. They concluded that the filament diameter exhibits greater deviation when the extrusion temperature is set at a non-optimal value.

3.2. Mechanical Properties

The mechanical properties of specimens printed with HIPS and rPS were analysed in terms of tensile strength, modulus, and elongation at break, as shown in Figures 4 and 5. The results indicated rPS exhibited higher tensile strength and modulus compared to HIPS. The specimens printed with rPS exhibited higher tensile strength (45.06 ± 4.31 MPa) and modulus (3127.22 ± 202.06 MPa) compared to HIPS (25.96 ± 1.53 MPa and 2356.90 ± 170.23 MPa), corresponding to increases of 73% and 33%, respectively. This difference can be explained by the material composition of HIPS, which contains rubber monomers to improve impact resistance while losing some of its stiffness and strength [10]. The rPS exhibits higher stiffness, as polystyrene is inherently more rigid and brittle due to the steric hindrance from its phenyl side groups, which significantly limit chain mobility and plastic deformation. This observation is also supported by the findings of Negash, Tatek, and Tsige [11]. Apart from differences in material properties, layer adhesion in 3D-printed parts is a critical factor that significantly affects their mechanical strength. In this study, rPS exhibited significantly better layer adhesion in the printed specimens compared to HIPS, as observed in the micrographs presented in Section 3.3. The enhanced layer bonding in the specimens printed with rPS resulted in significantly higher tensile strength and modulus compared to those printed with HIPS.

As shown in Figure 5, specimens printed with rPS exhibited greater elongation at break (3.46 ± 0.56%) compared to specimens printed with HIPS (1.71 ± 0.19%). This finding is somewhat unexpected, as HIPS is typically engineered for better toughness. The results reported in section 3.3 also indicated that HIPS is a ductile material. Moreover, Ng et al. [5] further supported this observation by comparing the tensile properties of specimens printed with HIPS and rPS. They found that specimens printed with HIPS exhibited greater elongation than those printed with rPS. As mentioned earlier, layer adhesion within the printed part is critical to its mechanical properties. This factor has a more dominant influence than the material properties themselves. As evidenced in Section 3.3, specimens printed with HIPS exhibited poorer layer adhesion compared to those printed with rPS. This weak interlayer bonding may lead to premature failure under tensile loading, causing the specimens to fracture at lower elongation levels. For this reason, the specimens printed with HIPS were less ductile than those printed with rPS, which contrasts with the findings reported in the literature.

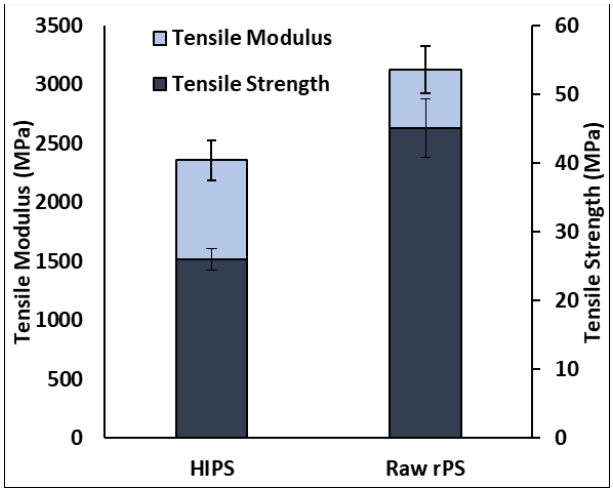

Figure 4. Tensile strength and modulus of specimens printed with commercial HIPS and rPS.

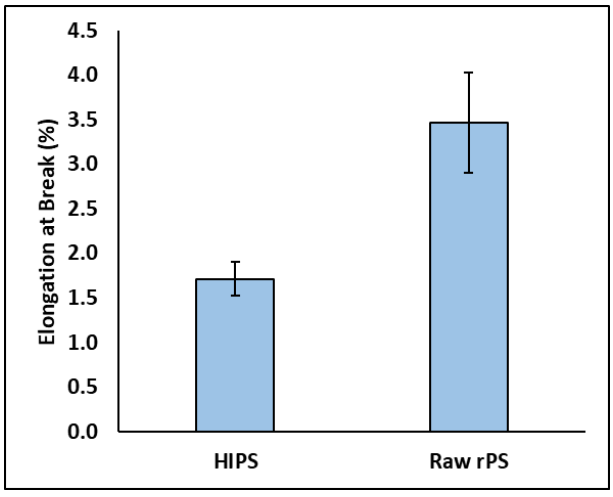

Figure 5. Elongation at break of specimens printed with commercial HIPS and rPS.

Figure 6 shows that specimens printed with HIPS exhibited higher impact strength (137.30 ± 16.63 J/m) compared to specimens printed with rPS (48.47 ± 9.38 J/m), absorbing nearly three times more energy before fracture, indicating it has better impact resistance. The large discrepancy is due to the material composition. The HIPS contains rubber particles dispersed in the polystyrene matrix, which act as stress concentrators that promote energy absorption through mechanisms like crazing, shear yielding, and rubber particle cavitation. These mechanisms allow HIPS to deform plastically rather than crack immediately under impact [12]. The rPS's brittleness, which causes rapid crack propagation with minimal energy absorption, is due to its higher stiffness. This stiffness comes from the molecular structure of polystyrene, where the steric hindrance provided by its bulky phenyl side groups severely restricts chain mobility and prevents plastic deformation.

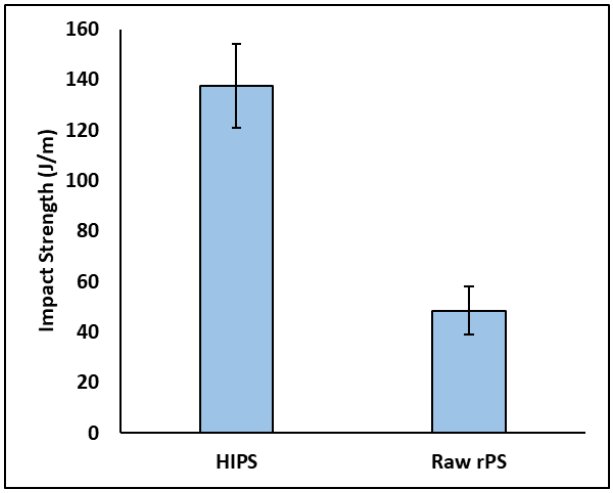

Figure 6. Impact strength of specimens printed with commercial HIPS and rEPS.

3.3. Morphological Properties

Figures 7 and 8 show SEM micrographs of fracture specimens printed with HIPS and rPS at 100 × and 800 × magnification. Under 100 × magnification, HIPS exhibits larger void gaps between layers, indicating poor layer adhesion. This is because HIPS contains rubber particles, which are added to enhance impact resistance. However, these rubber domains can hinder polymer chain diffusion during printing, leading to weak layer adhesion and larger voids. Additionally, HIPS has higher thermal shrinkage than rPS due to its rubber-modified structure. During cooling, this creates stress at the layer interfaces, pulling them apart and causing poor layer adhesion [13]. In contrast, rPS demonstrates more homogeneous flow and better layer adhesion, as no noticeable gaps are observed between the printed layers due to the absence of rubber monomers.

These morphological results correlate with the tensile properties discussed in Section 3.2. The good layer adhesion in rPS specimens contributes to their higher tensile strength and modulus, as the well-bonded layers distribute stress more effectively under tensile load. Conversely, the weak interlayer adhesion in HIPS specimens leads to premature failure under tensile stress, resulting in poor tensile properties despite HIPS's inherent ductility. This explains the unexpected finding that rPS exhibited greater elongation at break than HIPS, as the latter's poor layer adhesion caused early fracture, overshadowing its material-level ductility. Thus, the morphological analysis highlights the critical role of layer adhesion in determining the tensile properties of 3D printed parts.

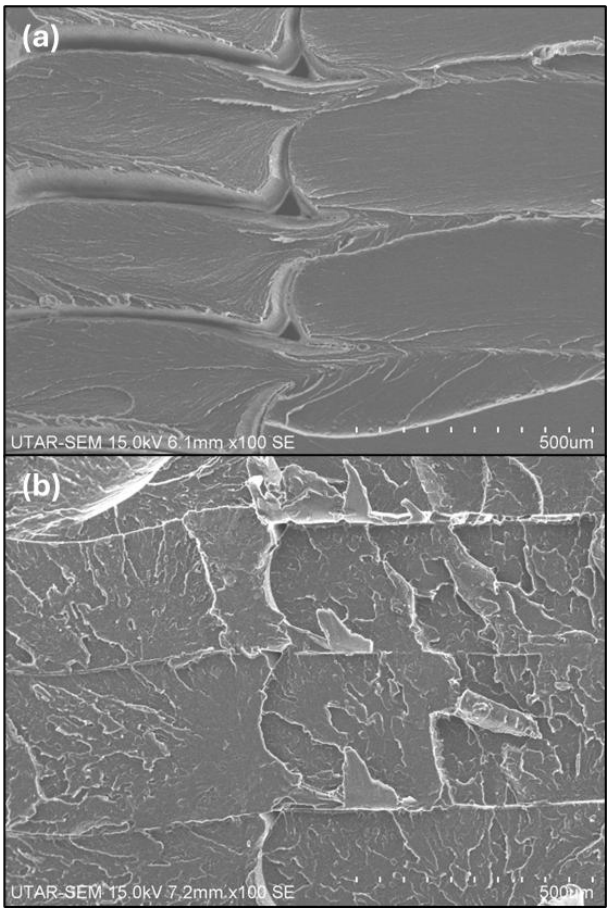

Figure 7. SEM micrographs of fracture specimens printed with (a) HIPS and (b) rPS at 100× magnification.

At 800 × magnification, fracture specimens printed with HIPS exhibit tearing behaviour due to the deformation and rupture of the dispersed rubber phases within the polystyrene matrix. When HIPS is subjected to stress, the rubber particles embedded in the matrix stretch significantly and eventually rupture, leaving behind fibrils, which are thin, elongated strands of rubber material that bridge cracks and help dissipate energy, thus toughening the material. The rPS appears smoother and flat fracture surface, suggesting brittle fracture. Brittle materials usually fracture with minimal plastic deformation, resulting in flat, smooth surfaces as observed in the SEM images, particularly at larger magnification. Polystyrene (PS) itself is brittle primarily due to the steric hindrance effect of the phenyl (styrene) groups attached to its polymer backbone. The bulky phenyl rings restrict the rotation and flexibility of the polymer chains, preventing them from sliding past one another under stress [14]. This rigidity limits the material's ability to deform plastically, as the steric hindrance inhibits energy-dissipating mechanisms like crazing or shear yielding. Instead of absorbing energy through gradual deformation, PS undergoes abrupt fracture when subjected to stress, resulting in smooth, flat fracture surfaces characteristic of brittle materials.

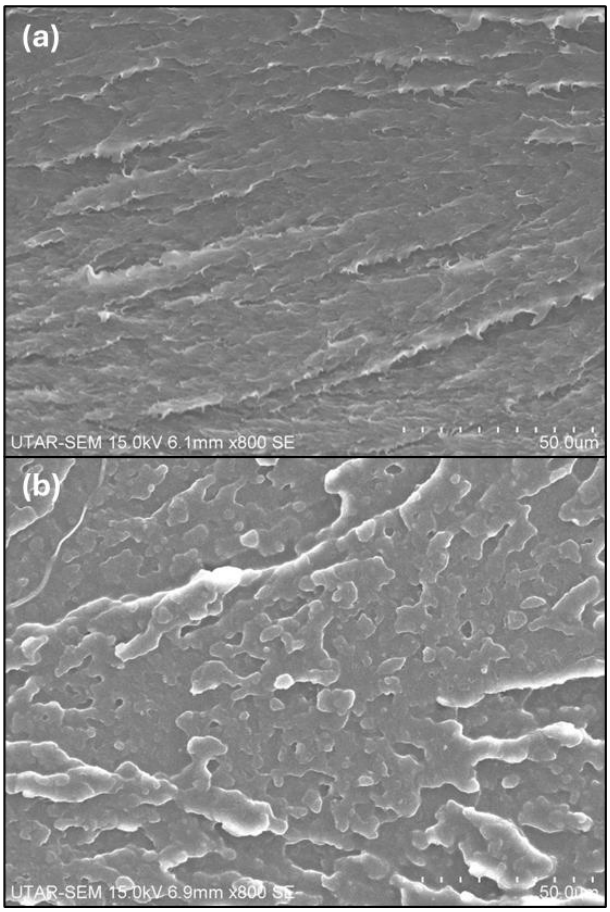

Figure 8. SEM micrographs of fracture specimens printed with (a) HIPS and (b) rPS at 800× magnification.

3.4. Thermal Properties

The thermal degradation behaviour of densified EPS, rPS filament, and HIPS filament was analysed using TGA. The TGA results, as shown in Figure 9, demonstrated that all three materials exhibit high thermal stability below 300°C, with minimal mass loss. However, beyond 300°C, rapid degradation occurs.

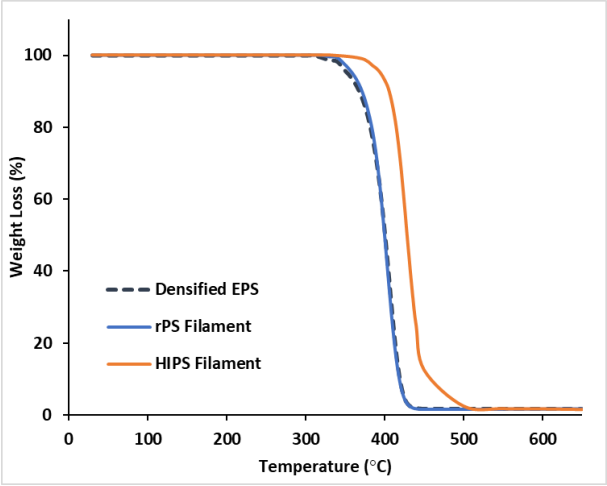

Figure 9. TGA results of Densified EPS, rPS filament, and HIPS filament.

The DTG curve in Figure 10 highlights that the densified EPS and rPS filament exhibit sharp, single-step degradation peaks at ~405°C. The thermal decomposition behaviour of rPS was similar to the findings reported by Ariel Leong et al. [14] and Ling et al. [15]. In contrast, the HIPS filament shows two distinct degradation peaks. The first peak appears at a lower temperature, corresponding to the decomposition of its rubber-modified components [16], while the second, more prominent peak occurs at approximately 429°C, reflecting the breakdown of its polystyrene matrix. This two-stage degradation process in HIPS results in a broader temperature range for

decomposition compared to the single-step degradation observed in densified EPS and rPS.

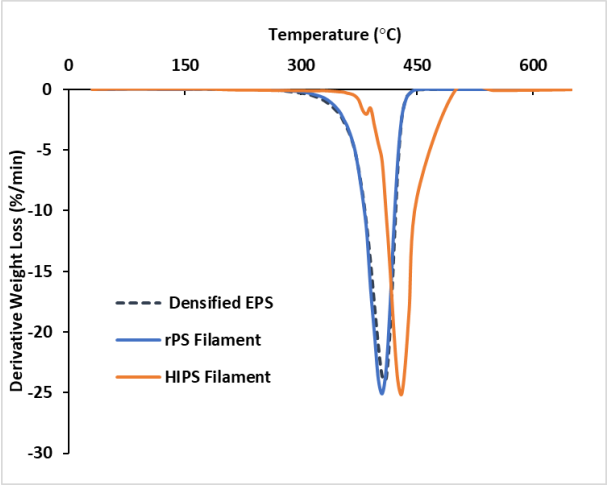

Figure 10. DTG results of Densified EPS, rPS filament, and HIPS filament.

The onset degradation temperature (T_d onset) obtained from the TGA curves and the maximum degradation temperature (T_d max) derived from the DTG curves are presented in Figure 11. The T_d onset and T_d max of densified EPS did not show significant changes after being processed into rPS pellets and subsequently extruded into rPS filament.

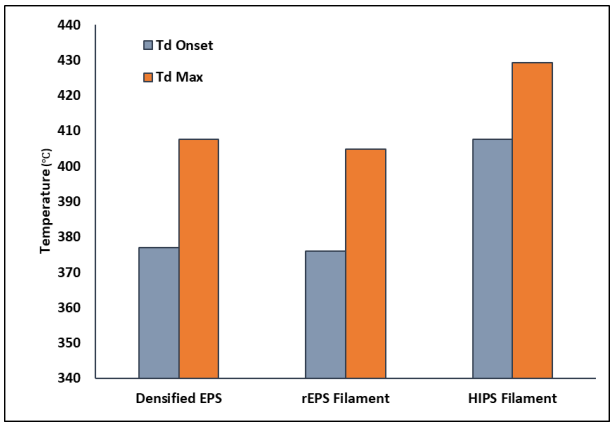

Figure 11. T_d Onset and T_d max results of Densified EPS, rPS filament, and HIPS filament.

Since the printing temperature is maintained below the T_d onset of rPS, it is unlikely to cause any printing issues related to thermal degradation. The HIPS filament exhibits a higher T_d onset and T_d max as compared to the rPS filament. HIPS exhibits better thermal stability than rPS due to its rubber-modified structure. The polybutadiene rubber phase absorbs energy and delays degradation, shifting the main polystyrene decomposition to a higher temperature [17]. These findings show HIPS is better suited for high-temperature applications.

CONCLUSION

This study demonstrated the feasibility of upcycling EPS waste into rPS filament for FFF 3D printing, offering a sustainable alternative to commercial HIPS. The extruded rPS filament achieved optimal diameter consistency, making it suitable for 3D printing. Specimens printed with rPS exhibited superior tensile strength, modulus, and elongation at break compared to HIPS because of better layer adhesion; however, HIPS demonstrated higher impact resistance due to its rubber-modified structure. Thermal analysis confirmed rPS's stability within printing temperatures, despite HIPS exhibiting greater thermal resistance. Morphological studies revealed brittle fracture in rPS and ductile tearing in HIPS, aligning with their mechanical behaviours. These findings highlight rPS's potential as a low-cost, sustainable, and functional 3D printing material for additive manufacturing, supporting circular economy initiatives while addressing EPS waste challenges.

ACKNOWLEDGMENTS

The authors acknowledge the financial support provided by the UTAR Research Fund (UTARRF) under project number IPSR/RMC/UTARRF/2025-C1/K03.

REFERENCES

[1] M. Enyan, J. N. O. Amu-Darko, E. Issaka, and O. J. Abban, "Advances in fused deposition modeling on process, process parameters, and multifaceted industrial application: a review," *Engineering Research Express*, vol. 6, no. 1, p. 012401, Mar. 2024, doi: 10.1088/2631-8695/ad32f6.

[2] S. Singh, G. Singh, C. Prakash, and S. Ramakrishna, "Current status and future directions of fused filament fabrication," *Journal of Manufacturing Processes*, vol. 55, pp. 288–306, Apr. 2020, doi: 10.1016/j.jmapro.2020.04.049.

[3] Grand View Research, Fused Deposition Modeling 3D Printing Market Size, Share & Trends Analysis Report By Printer Type (Desktop, Industrial), By Application, By End-use, By Region, And Segment Forecasts, 2024 - 2030. 2024. [Online]. Available: https://www.grandviewresearch.com/industry-analysis/fused-deposition-modeling-3d-printing-market-report.

[4] J. S. Chu, S. C. Koay, M. Y. Chan, H. L. Choo, and T. K. Ong, "Recycled plastic filament made from post-consumer expanded polystyrene and polypropylene for fused filamant fabrication," *Polymer Engineering and Science*, vol. 62, no. 11, pp. 3786–3795, Oct. 2022, doi: 10.1002/pen.26144.

[5] T. Y. Ng, S. C. Koay, M. Y. Chan, H. L. Choo, and T. K. Ong, "Preparation and characterisation of 3D printer filament from post-used styrofoam," *AIP Conference Proceedings*, Jan. 2020, doi: 10.1063/5.0001340.

[6] INTCO Recycling, "How To Recycle EPS," *GREEN MAX INTCO Recycling*, 2024. https://www.intcorecycling.com/How-to-recycle-eps.html.

[7] C. Abeykoon, P. Pérez, and A. L. Kelly, "The effect of materials' rheology on process energy consumption and melt thermal quality in polymer extrusion," *Polymer Engineering and Science*, vol. 60, no. 6, pp. 1244–1265, Apr. 2020, doi: 10.1002/pen.25377.

[8] S. Hamat, Ishak, S. M. Sapuan, N. Yidris, Hussin, and A. Manan, "Influence of filament fabrication parameter on tensile strength and filament size of 3D printing PLA-3D850," *Materials Today Proceedings*, vol. 74, pp. 457–461, Nov. 2022, doi: 10.1016/j.matpr.2022.11.145.

[9] V. Senkerik, M. Bednarik, V. Janostik, M. Karhankova, and A. Mizera, "Analysis of extrusion process parameters in PLA filament production for FFF Technology," *MANUFACTURING TECHNOLOGY*, vol. 24, no. 2, pp. 265–271, Apr. 2024, doi: 10.21062/mft.2024.037.

[10] J. Rovere, C. A. Correa, V. G. Grassi, and M. F. D. Pizzol, "Role of the rubber particle and polybutadiene cis content on the toughness of high impact polystyrene," Journal of Materials Science, vol. 43, no. 3, pp. 952–959, Nov. 2007, doi: 10.1007/s10853-007-2197-2.

[11] S. Negash, Y. B. Tatek, and M. Tsige, "Effect of tacticity on the structure and glass transition temperature of polystyrene adsorbed onto solid surfaces," *The Journal of Chemical Physics*, vol. 148, no. 13, Apr. 2018, doi: 10.1063/1.5010276.

[12] Alfarraj, A., & Nauman, E. B. (2004). Super HIPS: improved high impact polystyrene with two sources of rubber particles. Polymer, 45(25), 8435–8442. https://doi.org/10.1016/j.polymer.2004.10.005.

[13] V. Serpooshan, S. Zokaei, and R. Bagheri, "Effect of rubber particle cavitation on the mechanical properties and deformation behavior of high-impact polystyrene," *Journal of Applied Polymer Science*, vol. 104, no. 2, pp. 1110–1117, Jan. 2007, doi: 10.1002/app.25633.

[14] J. J. Arieal Leong, S. C. Koay, M. Y. Chan, H. L. Choo, K. Y. Tshai, and T. K. Ong, "Composite filament made from post-used Styrofoam and corn husk fiber for fuse deposition modeling," *Journal of Natural Fibers*, vol. 19, no. 13, pp. 7033-7048, Jun, 2021, doi: 10.1080/15440478.2021.1941488.

[15] S. L Ling, S. C. Koay, M. Y. Chan, K. Y. Thsai, T. R. Chantara, and M. M. Pang, "Wood plastic composites produced from postconsumer recycled polystyrene and coconut shell: effect of coupling agent and processing aid on tensile, thermal, and morphological properties," *Polymer Engineering and Science*, vol. 60, no. 1, pp. 202-210, Jan. 2020, doi: 10.1002/pen.25273.

[16] A. Hejna, M. Marć, P. Szymański, K. Mizera, and M. Barczewski, "Analysis of emission of volatile organic compounds and thermal degradation in investment casting using fused deposition modeling (FDM) and three-dimensional printing (3DP) made of various thermoplastic polymers," *Environmental Science and Pollution Research*, vol. 31, no. 50, pp. 60371–60388, Oct. 2024, doi: 10.1007/s11356-024-35200-x.

[17] S. P. Thomas, "Polystyrene-Based composites and their toughening mechanisms," in *CRC Press eBooks*, 2022, pp. 15–27. doi: 10.1201/9780429330575-2.